Article

Structure/Reactivity Studies on an #-Lithiated Benzylsilane: Chemical Interpretation of Experimental Charge Density

Holger Ott, Christian Da#schlein, Dirk Leusser, Daniel Schildbach, Timo Seibel, Dietmar Stalke, and Carsten Strohmann

J. Am. Chem. Soc., **2008**, 130 (36), 11901-11911 • DOI: 10.1021/ja711104q • Publication Date (Web): 15 August 2008

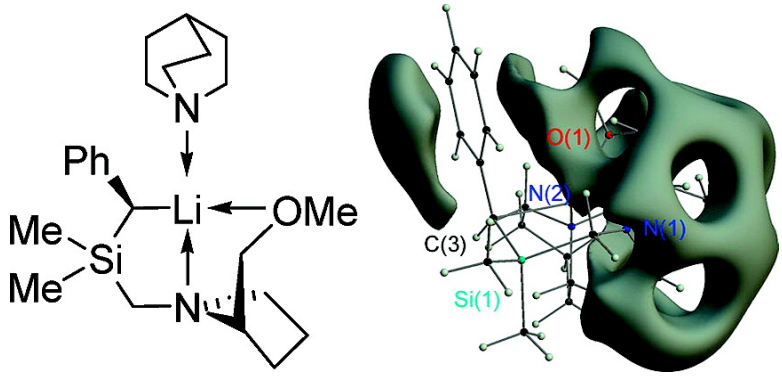

More About This Article

Additional resources and features associated with this article are available within the HTML version:

- Supporting Information
- Access to high resolution figures
- Links to articles and content related to this article
- Copyright permission to reproduce figures and/or text from this article

View the Full Text HTML

J|A|C|S
ARTICLES

Published on Web 08/15/2008

Structure/Reactivity Studies on an α-Lithiated Benzylsilane: Chemical Interpretation of Experimental Charge Density

Holger Ott,[†] Christian Däschlein,[‡] Dirk Leusser,[†] Daniel Schildbach,[‡] Timo Seibel,[‡] Dietmar Stalke,[†] and Carsten Strohmann*,[‡]

Institut für Anorganische Chemie, Universität Göttingen, Tammannstrasse 4, 37077 Göttingen, Germany, and Institut für Anorganische Chemie, Universität Würzburg, Am Hubland, 97074 Würzburg, Germany

Received December 19, 2007; E-mail: mail@carsten-strohmann.de

Abstract: Modern organic synthesis (e.g., of natural products) is virtually impossible without employment of enantiomerically enriched compounds. In many cases, alkyllithium compounds are key intermediates for the generation of these stereogenic substances. In recent years, the lithiated carbon atom in silicon-substituted benzyllithium compounds has become a focus of interest because it is possible to maintain its stereogenic information. Starting from a highly enantiomerically enriched benzylsilane, (*R*,*S*)-**2**·quinuclidine could be obtained, and the absolute configuration at the metalated carbon atom was determined by X-ray diffraction analysis. In solution, a quartet was found in the ^{13}C NMR spectrum for the metalated carbon atom because of coupling between carbon and lithium, indicating a fixed lithium carbon contact at room temperature. After reaction of (*R*,*S*)-**2**·quinuclidine with trimethylchlorostannane, the trapped product (*S*,*S*)-**4** was obtained with a dr ≥ 98:2 with inversion of the configuration at the metalated carbon. Multipole refinement against high-resolution diffraction data and subsequent topological analysis of the benchmark system (*R*,*S*)-**2**·quinuclidine provide insight in the electronic situation and thus the observed stereochemical course of the transformations. Surprisingly, the negative charge generated at the carbanion hardly couples into the phenyl ring. The neighboring silicon atom counterbalances this charge by a pronounced positive charge. Therefore, the α-effect of the silicon atom is caused not just by a polarization of the electron density but also by an electrostatic bond reinforcement. Furthermore, the experimentally determined electrostatic potential unequivocally explains the observed back side attack of an electrophile under inversion of the stereogenic center with high diastereomeric ratios.

Introduction

The synthesis of enantiomerically or diastereomerically enriched alkyllithium compounds,[1] in which the metalated carbon atom is a stereogenic center, has been studied vigorously for more than 20 years.[2] In general, they have been synthesized in deprotonation reactions employing strong alkyllithium bases such as butyllithium. Although the configuration of the metalated stereogenic carbon atom is stable only at low temperatures (−78 °C) for most of these compounds, Hoppe et al. and Strohmann et al. were able to characterize key compounds that proved to have a stable configuration at higher temperatures for at least minutes.[2,3] A frequently proposed mechanism for the racemization implies a planar sp^2-hybridized intermediate carbanion (**C**), which proceeds via a separated ion pair (**B** and *ent*-**B**) in Scheme 1.

Although this racemization process occurs fast at low temperatures in polar solvents, there are three main strategies to increase the configurational stability of the lithiated species (shown in the lower part of Scheme 1). The first ideas involved the introduction of an *electronegative substituent* in α-position to the negative charge to raise the inversion barrier (ii).[4a] According to Bent's rule,[5] the electronegative substituent in **E** increases the p-character of the corresponding bond, raises the energy barrier to achieve the planar transition state (∼35

[†] Universität Göttingen.
[‡] Universität Würzburg.

(1) In general, we speak of enantiomerically enriched metal alkyls if we focus our interest on the stereogenic metalated carbon atom, whereas these molecules are almost always diastereomerically enriched metal alkyls, because of the presence of more stereogenic centers than only the metalated one.

(2) (a) Chan, T. H.; Pellon, P. J. *J. Am. Chem. Soc.* **1989**, *111*, 8737–8738. (b) Chan, T. H.; Lamonthe, S. *Tetrahedron Lett.* **1991**, *32*, 1847–1850. (c) Chan, T. H.; Nwe, K. T. *J. Org. Chem.* **1992**, *57*, 6107–6111. (d) Hoppe, D.; Hense, T. *Angew. Chem.* **1997**, *109*, 2376−2410; *Angew. Chem., Int. Ed. Engl.* **1997**, *36*, 2282−2316. (e) Beak, P.; Anderson, D. R.; Curtis, M. D.; Laumer, J. M.; Pippel, D. J.; Weisenburger, G. A. *Acc. Chem. Res.* **2000**, *33*, 715–727. (f) Basu, A.; Thayumanavan, S. *Angew. Chem.* **2002**, *114*, 740−763; *Angew. Chem., Int. Ed.* **2002**, *41*, 716−738 and references therein. (g) Hoppe, D.; Marr, F.; Brüggemann, M. Enantioselective synthesis by lithiation adjacent to oxygen and electrophile incorporation. In *Organolithiums in enantioselective synthesis*; Hodgson, D. M., Ed.; Topics in Organometallic Chemistry; Springer-Verlag: Berlin, 2003; Vol. 5, pp 61−138. (h) Beak, P.; Johnson, T. A.; Kim, D. D.; Lim, S. H. Enantioselective synthesis by lithiation adjacent to nitrogen and electrophile incorporation. In *Organolithiums in enantioselective synthesis*; Hodgson, D. M., Ed.; Topics in Organometallic Chemistry; Springer-Verlag: Berlin, 2003; Vol. 5, pp 139−176. (i) Gawley, R. E.; Coldham, I. Alpha-amino-organolithium compounds. In *The chemistry of organolithium compounds*; Rappoport, Z., Marek, I., Eds.; Wiley & Sons: Chichester, 2004; pp 997−1053. (j) Hoppe, D.; Christoph, G. Asymmetric deprotonation with alkyllithium-(−)-sparteine. In *The chemistry of organolithium compounds*; Rappoport, Z., Marek, I., Eds.; Wiley & Sons: Chichester, 2004; pp 1055−1164.

Scheme 1. Racemization Process of Alkyllithium Compounds **A** to *ent*-**A** and Possible Approaches To Increase the Inversion Barrier[2a,b,3d,f,h,4]

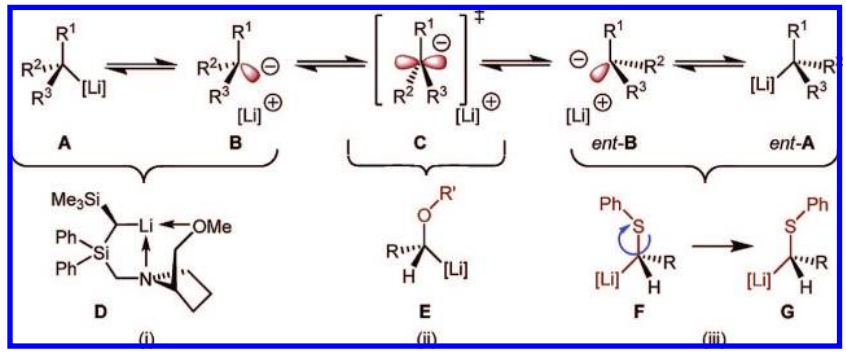

kJmol^{-1}), and thus hinders the racemization. A second approach is based on the introduction of an *organosulfane substituent* in the α-position to the negative charge, mainly propagated by Hoffmann et al. (iii).[4b] Now, in addition to the inversion, a rotation about the C−S bond would be required for racemization (**F** to **G**). This rotation is the rate-determining step of the whole process with an activation energy of about 50 kJ mol^{-1}, because negative hyperconjugation[6] stabilizes the negative charge at the carbanionic center. A third approach is the strong fixation of the metal to the carbon atom by "*side-arm complexation*" based on Klumpps' idea of oxygen- and nitrogen-assisted lithiation (i).[7] This fixation, also used by Chan et al. and our own group,[2a,b,3d,f,h] leads to an increased inversion barrier of carbanionic systems such as **D** of about 100−120 kJ mol^{-1}.

For several years, these compounds have been the subject of discussion concerning the complete stereochemical course of their formation through deprotonation[8] and the trapping reactions with different electrophiles such as carbonyl reagents or group 14 halides (e.g., alkyl-, silyl-, and stannyl halides). The determination of the absolute configuration at the metalated stereogenic center and the clarification of the stereochemical course of further transformations are of major interest.[9] To determine absolute configurations, single-crystal X-ray diffraction provides the most unambiguous assignments, but only limited information is available for the corresponding alkyllithium compounds, because they are thermally unstable and sensitive to hydrolysis.[3d,f,h,10]

In 1994, Carstens and Hoppe[11a] reported several examples of the reaction of a highly enantiomerically enriched benzyllithium compound with different electrophiles. In contrast to nonmesomerically stabilized sp^3-hybridized organolithium compounds that react with almost all electrophiles under strict stereoretention, the reaction of these systems with electrophiles can result in either retention or inversion of the absolute configuration at the stereogenic carbon atom, depending on the attack of the electrophile from the front side or the back side of the metalated atom. Most of the trapping reactions occur with inversion (alkyl-, silyl-, and stannyl halides, acid chlorides, carbon dioxide, carbon disulfide, and alkylisocyanates), and only the reactions with protic acids, aliphatic aldehydes, ketones, or esters as electrophiles occur with retention.[2j]

What are the reasons for the preference of stereoinversion and for the observed retention in reactions with carbonyl compounds and group 14 halides? Assuming that intermediates with precomplexed electrophiles compete with direct substitution, the electrophile should have a significant influence on the stereochemical course. Electrophiles that are capable of strong coordination to the lithium atom, such as carbonyl compounds, yield products with retention of the configuration. Electrophiles that are not able to precoordinate to the lithium atom yield products mainly with inversion of the configuration by attacking the vacant "back side". In some cases, unfavorable steric interactions interfere with the inversion process and lead to the retention product.[2f] In addition to the influence of the electrophile employed, it is obvious that the substitution and geometry of the carbanionic atom has a crucial influence on the reaction pathway. If the carbanion is planar, the reaction with the

(3) (a) Kaiser, B.; Hoppe, D. *Angew. Chem.* **1995**, *107*, 344−346; *Angew. Chem., Int. Ed. Engl.* **1995**, *34*, 323−325. (b) Hoppe, D.; Kaiser, B.; Stratmann, O.; Fröhlich, R. *Angew. Chem.* **1997**, *109*, 2872−2874; *Angew. Chem., Int. Ed. Engl.* **1997**, *36*, 2784−2786. (c) Marr, F.; Fröhlich, R.; Hoppe, D. *Org. Lett.* **1999**, *1*, 2081–2083. (d) Strohmann, C.; Lehmen, K.; Wild, K.; Schildbach, D. *Organometallics* **2002**, *21*, 3079–3081. (e) Strohmann, C.; Buchhold, D. H. M.; Seibel, T.; Wild, K.; Schildbach, D. *Eur. J. Inorg. Chem.* **2003**, 3453–3463. (f) Strohmann, C.; Abele, B. C.; Lehmen, K.; Villafane, F.; Sierra, L.; Martín-Barrios, S.; Schildbach, D. *J. Organomet. Chem.* **2002**, *661*, 149–158. (g) Strohmann, C.; Seibel, T.; Schildbach, D. *J. Am. Chem. Soc.* **2004**, *126*, 9876–9877. (h) Strohmann, C.; Abele, B. C.; Lehmen, K.; Schildbach, D. *Angew. Chem.* **2005**, *117*, 3196−3199; *Angew. Chem., Int. Ed.* **2005**, *44*, 3136−3139. (i) Strohmann, C.; Lehmen, K.; Dilsky, S. *J. Am. Chem. Soc.* **2006**, *128*, 8102–8103.

(4) (a) Still, W. C.; Sreekumar, C. *J. Am. Chem. Soc.* **1980**, *102*, 1201–1202. (b) Dress, R. K.; Rölle, T.; Hoffmann, R. W. *Chem. Ber.* **1995**, *128*, 673–677.

(5) Bent, H. A. *Chem. Rev.* **1961**, *61*, 275–311.

(6) (a) Reed, A. E.; Schleyer, P. v. R. *J. Am. Chem. Soc.* **1990**, *112*, 1434–1445. (b) Salzner, U.; Schleyer, P. v. R. *J. Am. Chem. Soc.* **1993**, *115*, 10231–10236. (c) Dobado, J. A.; Martínez-Garzía, H.; Molina, J. M.; Sundberg, M. R. *J. Am. Chem. Soc.* **1998**, *120*, 8461–8471. (d) Stefan, T.; Janoschek, R. *J. Mol. Model.* **2000**, *6*, 282–288.

(7) Review: Klumpp, G. W. *Recl. Trav. Chim. Pays-Bas* **1986**, *105*, 1–21.

(8) Review on CIPE: Whisler, M. C.; MacNeil, S.; Snieckus, V.; Beak, P. *Angew. Chem.* **2004**, *116*, 2256−2276; *Angew. Chem., Int. Ed.* **2004**, *43*, 2206−2225.

(9) (a) Current results concerning the topic of transformations of lithiated stereogenic centers: Strohmann, C.; Däschlein, C.; Kellert, M.; Auer, D. *Angew. Chem.* **2007**, *119*, 4864−4866; *Angew. Chem., Int. Ed.* **2007**, *46*, 4780. (b) Strohmann, C.; Däschlein, C.; Auer, D. *J. Am. Chem. Soc.* **2006**, *128*, 704–705.

(10) (a) Ahlbrech, H.; Boche, G.; Harms, K.; Marsch, M.; Sommer, H. *Chem. Ber.* **1990**, *123*, 1853–1858. (b) Papasergio, R. I.; Skelton, B. W.; Twiss, P.; White, A. H.; Raston, C. L. *J. Chem. Soc., Dalton Trans.* **1990**, 1161–1172. (c) Marsch, M.; Harms, K.; Zschage, O.; Hoppe, D.; Boche, G. *Angew. Chem.* **1991**, *103*, 338−339; *Angew. Chem., Int. Ed. Engl.* **1991**, *30*, 321−323. (d) Boche, G.; Marsch, M.; Harbach, J.; Harms, K.; Ledig, B.; Schubert, B.; Lohrenz, J. C. W.; Ahlbrecht, H. *Chem. Ber.* **1993**, *126*, 1887–1894. (e) Hoppe, I.; Marsch, M.; Harms, K.; Boche, G.; Hoppe, D. *Angew. Chem.* **1995**, *107*, 2328−2330; *Angew. Chem., Int. Ed. Engl.* **1995**, *34*, 2158−2160.

(11) (a) Carstens, A.; Hoppe, D. *Tetrahedron* **1994**, *50*, 6097–6108. (b) Derwing, C.; Frank, H.; Hoppe, D. *Eur. J. Org. Chem.* **1999**, 3519–3524.

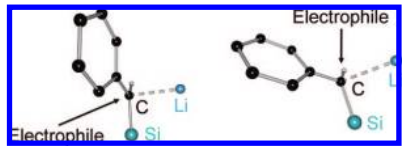

Figure 1. Preferred reaction of an electrophile with a *planar carbanion* from the *back side* causes inversion (left), and preferred reaction of an electrophile with a *pyramidalized carbanion* from the *front side* causes retention (right).

electrophile can occur from the less hindered, uncoordinated back side of the molecule to cause inversion. If the carbanionic center is pyramidalized, retention should be preferred as a consequence of the easier access to the front side of the molecule (Figure 1).

Along with this geometrically imposed behavior of the carbanion, there is an electronic reason for the preferred stereoretention of pyramidalized compounds and the stereoinversion with planar compounds, first pointed out by Carstens and Hoppe.[11a] Increased planarization increases the electron density at the back side to the Li−C bond and therefore the attractivity for an approaching electrophile to interact with that side of the molecule. Especially electrophiles that have a low-energy LUMO do react rapidly with these carbanions through an invertive pathway (orbital-controlled reaction).[2f]

Although all these effects are very important to rationalize the suggested reaction patterns of benzyllithium compounds, the coordination sphere of the lithium atom has not attracted much interest yet.[12] In 2005, we reported on a highly diastereomerically enriched silyl-substituted alkyllithium compound.[3h] Substitution occurs under retention or inversion, determined by an open or blocked coordination side at the lithium atom, respectively. If the reaction is carried out in noncoordinating toluene/cyclohexane solution, one coordination side of the lithium atom remains vacant and the trialkyl stannyl chloride is able to precoordinate. The reaction follows the retentive pathway (dr = 91:9). If THF is coordinated to the lithium atom, precoordination of the electrophile is impossible and the attack occurs from the back side of the molecule, causing inversion (dr = 92:8). With regard to this reaction, it is important to note that it is normally impossible to perform those reactions with high diastereomeric excess if THF is used as the parent solvent, because this would generate solvent-separated ion pairs (SSIP) with no defined stereochemical information.

This interesting dependence on the stereochemical course of the trapping reaction by varying the solvent showed that the coordination sphere of the lithium atom must be considered to understand these reaction sequences.[13] Additional work on the planar, highly diastereomerically enriched benzyllithium compound (*R*,*S*)-**2** showed that the reaction of this compound with electrophiles took place mainly with inversion of the absolute configuration. The trapping reaction (e.g., with methyl iodide) yielded the inversion product (*S*,*S*)-**3** (Scheme 2).[3f] It was even possible to use diethyl ether or a mixture of toluene and 1 equiv of THF as solvents to get the dr of the reaction sequence; only parent THF as the solvent lowered the dr. As long as the contact

Scheme 2. Synthesis and Trapping Reaction of the Highly Diastereomerically Enriched Benzyllithium Compound (*R*,*S*)-**2**·DABCO[a]

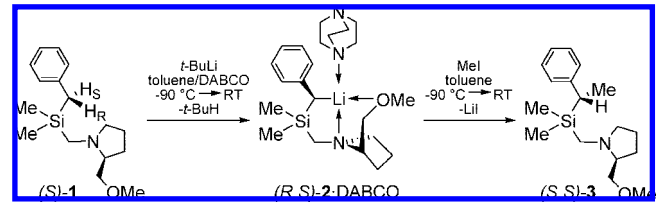

[a] The deprotonation reaction yielded in the *R*-configurated carbanion, while the nucleophilic attack of methyl iodide proceeded with inversion of the absolute configuration at the former carbanion.

Scheme 3. Synthesis of the Highly Diastereomerically Enriched Benzyllithium Compound (*R*,*S*)-**2**·Quinuclidine

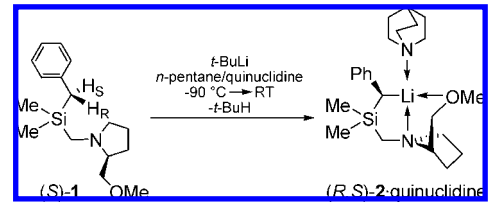

ion pair (CIP) stays intact, the donor solvent should not matter (THF with a dipole moment of $\mu = 1.75$ [D] has a stronger donor capacity compared to that of Et_2O ($\mu = 1.15$ [D])[14]), but if a strong donor generates an SSIP the dr drops considerably. Additionally, it has to be mentioned that the presence of the lithium-donating diamine DABCO[3e] (and in the present study the quinuclidine molecule) is not necessary for the stereoselectivity, but is required to obtain high quality single crystals.

As part of our studies on diastereomerically enriched alkyllithium compounds, we synthesized the highly diastereomerically enriched benzyllithium compound (*R*,*S*)-**2**·quinuclidine. Its trapping with trimethylchlorostannane resulted in the formation of the highly diastereomerically enriched compound **9** (dr 98:2). The absolute configuration of both compounds could be determined by X-ray structural analysis (in case of **9** as the methyl iodide derivative). Because the crystals obtained of (*R*,*S*)-**2** quinuclidine have a high-quality, high-resolution X-ray diffraction analysis was performed to determine the electron density distribution from experimental data. Topological analyses were employed to answer the most important questions concerning this compound: (i) Where is the electron density and hence the negative charge of the carbanion localized? (ii) Which consequence has the planar stereogenic center in compound (*R*,*S*)-**2** to the electron (re)distribution and therefore the stereochemical pathway of the reaction? (iii) What is the nature of the Li−C bond?

Results and Discussion

Synthesis of (*R*,*S*)-2·Quinuclidine. (*R*,*S*)-**2**·quinuclidine was synthesized by lithiation of the enantiomerically pure starting material (*S*)-**1** with *tert*-butyllithium in *n*-pentane in the presence of 1 equiv of quinuclidine at −90 °C (Scheme 3) to give an immediate precipitation of a yellow solid. After warming to room temperature, the yellow solid was redissolved by adding a little toluene and then stored at −30 °C. After 24 h, yellow crystals were obtained. Obviously, it cannot be decided whether

(12) (a) Fraenkel, G.; Martin, K. V. *J. Am. Chem. Soc.* **1995**, *117*, 10336–10344. (b) Fraenkel, G.; Chow, A.; Fleischer, R.; Liu, H. *J. Am. Chem. Soc.* **2004**, *126*, 3983–3995. (c) Fraenkel, G.; Gallucci, J.; Liu, H. *J. Am. Chem. Soc.* **2006**, *128*, 8211–8216.

(13) (a) For ligand effects, see for example: Ramírez, A.; Lobkovsky, E.; Collum, D. B. *J. Am. Chem. Soc.* **2003**, *125*, 15376–15387. (b) Chadwick, S. T.; Ramírez, A.; Gupta, L.; Collum, D. B. *J. Am. Chem. Soc.* **2007**, *129*, 2259–2268.

(14) *CRC Handbook of Chemistry and Physics*, 87th ed.; Lide, D. R., Ed., Taylor & Francis: Boca Raton, FL, 2006.

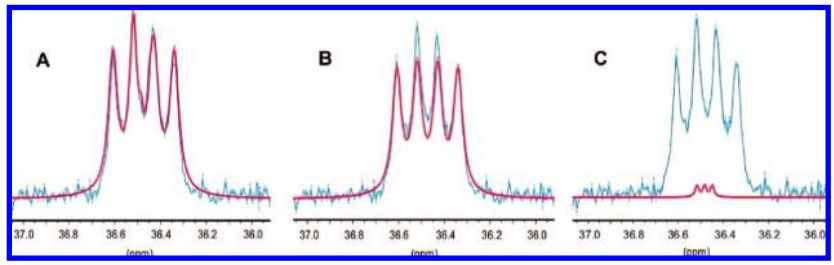

Figure 2. Section of the ^{13}C NMR spectrum of (*R*,*S*)-**2**·quinuclidine. Blue line shapes: experimental $^{13}C-Li$ coupling. Red line shapes: simulated $^{13}C-Li$ coupling. (A) $^{13}C-^{7}Li$ and $^{13}C-^{6}Li$ coupling add up. (B) $^{13}C-^{7}Li$ coupling. (C) $^{13}C-^{6}Li$ coupling.

(*R*,*S*)-**2**·quinuclidine is a kinetically controlled deprotonation product or a thermodynamically controlled crystallization product.

^{13}C NMR Studies of (*R*,*S*)-2·Quinuclidine. ^{13}C NMR spectra were recorded to gain information about the configurational stability of the lithiated carbon atom. On the basis of the observed $^{13}C-^{7}Li$ coupling at room temperature in toluene-d_8, (*R*,*S*)-**2**·quinuclidine should have at least a stable configuration on the NMR timescale at room temperature and therefore on the reaction timescale at −78 °C. Moreover, the ^{13}C NMR spectrum of (*R*,*S*)-**2**·quinuclidine shows only one set of signals, indicating the presence of only one diastereomer. The resonance signal for the metalated carbon atom is observed at 36.5 ppm. The signal consists of a quartet (nuclear spin of $^{7}Li/I = 3/2$; $^{13}C-^{7}Li$ coupling: 9 Hz), indicating only one fixed C−Li contact in solution, thus representing a monomer.

A quartet with four equal peaks is expected for a $^{13}C-^{7}Li$ coupling. The observed signal form is not symmetric, which can be caused by an overlap with the corresponding signal of the second possible diastereomer (*S*,*S*)-**2**·quinuclidine or by the $^{13}C-^{6}Li$ coupling (natural abundance $^{7}Li/^{6}Li \approx 92.5:7.5\%$). To rationalize the shape, the $^{13}C-Li$ coupling was simulated (Figure 2). Figure 2A shows the superimposed simulated spectra of the $^{13}C-^{7}Li$ and $^{13}C-^{6}Li$ coupling, Figure 2B shows the same for the $^{13}C-^{7}Li$ coupling, and Figure 2C shows the $^{13}C-^{6}Li$ coupling. In all three cases, the red line refers to the simulated spectrum and the blue line to the experimental. Obviously, the experimental line shape of the nonsymmetric quartet is a result of the coupling between ^{13}C and ^{6}Li (C). The addition of the symmetric line shape of the simulated $^{13}C-^{7}Li$ coupling (B) results in the observed experimental shape (A = B + C).

Molecular Structure in the Crystal of (*R*,*S*)-2·quinuclidine. The yellow single crystals we obtained were suitable for experimental charge density investigations. (*R*,*S*)-**2**·quinuclidine crystallizes from *n*-pentane/toluene in the chiral orthorhombic space group $P2_12_12_1$ (Figure 3 and Table 1) as rhombohedral blocks. The absolute structure could be determined unambiguously on the basis of the known configuration of C(14). The refinement of the Flack *x* parameter to 0.01(3) additionally confirmed the assignment of the stereoisomer.[15]

The asymmetric unit contains one molecule of (*R*,*S*)-**2**·quinuclidine. The slightly distorted tetrahedral coordination polyhedron of the lithium atom arises from contacts to the benzylic carbon atom, to the (methoxymethyl)pyrrolidine side-arm oxygen and nitrogen atom and to the nitrogen atom of the quinuclidine molecule. As anticipated, the side arm keeps the lithium atom in a fixed position.[16] The (*R*)-configured stereogenic carbon atom C(3) shows almost planar coordination with respect to the three next neighboring atoms (358° sum of bond angles). The lithium−carbon bond length of 2.273 Å is in the expected range.[17] The Si(1)−C(3) bond length of 1.813 Å is clearly shortened compared to, for example, Si(1)−C(10) of 1.907 Å (standard Si−C bond length: 1.87 Å).[18] This is normally attributed to the α-stabilizing effect of the silicon atom to a metalated carbon atom. Furthermore, the phenyl substituent seems to have a stabilizing effect on the metalated carbon atom. Starting from the metalated carbon atom as a carbanion, four

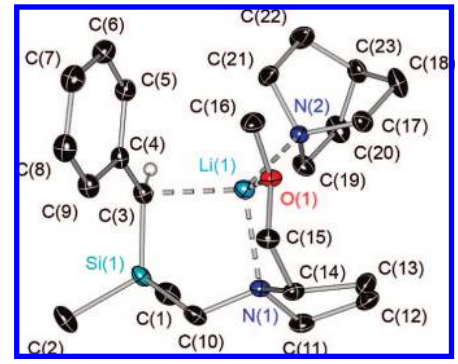

Figure 3. Molecular structure of (*R*,*S*)-**2**·quinuclidine in the solid state. Hydrogen atoms except the benzylic one are omitted for clarity. Anisotropic displacement parameters are depicted at the 50% probability level. Selected bond lengths (Å) and angles (deg): Si(1)−C(3), 1.8131(4); Si(1)−C(10), 1.9070(4); Li(1)−C(3), 2.2725(6); Li(1)−O(1), 1.9820(6); Li(1)−N(1), 2.1618(5); Li(1)−N(2), 2.1180(5); C(3)−C(4), 1.4343(4); C(4)−C(5), 1.4272(5); C(5)−C(6), 1.3859(5); C(6)−C(7), 1.3947(6); C(7)−C(8), 1.3992(6); C(8)−C(9), 1.3902(5); C(4)−C(9), 1.4266(4); C(3)−Si(1)−C(10), 108.560(14); C(4)−C(5)−C(6), 123.05(3); C(5)−C(4)−C(9), 114.22(3); C(5)−C(6)−C(7), 121.19(4); C(6)−C(7)−C(8), 117.59(3); C(7)−C(8)−C(9), 121.49(3); C(4)−C(9)−C(8), 122.45(3).

(15) Flack, H. D. *Acta Crystallogr.* **1983**, *A39*, 876–881.

(16) Ph_3C^- and $PyPh_2C^-$ are elucidative examples for side-arm fixation. While the alkali metals shift from the central deprotonated carbon atom toward the ring center of a single phenyl substituent as their mass gets bigger (Hoffmann, D.; Bauer, W.; Schleyer, P. v. R.; Pieper, U.; Stalke, D. *Organometallics* **1993**, *12*, 1193−1200), the pyridyl ring nitrogen atom keeps them in a fixed position (Pieper, U.; Stalke, D. *Organometallics* **1993**, *12*, 1201−1206).

(17) (a) For example, *t*BuLi and *n*BuLi: Kottke, T.; Stalke, D. *Angew. Chem.* **1993**, *105*, 619−621; *Angew. Chem., Int. Ed. Engl.* **1993**, *32*, 580. (b) Review: Stey, T.; Stalke, D. Lead structures in lithium organic chemistry. In *The chemistry of organolithium compounds*; Rappoport, Z., Marek, I., Eds.; Wiley & Sons: Chichester, 2004; pp 47−120. (c) Strohmann, C.; Seibel, T.; Strohfeldt, K. *Angew. Chem.* **2003**, *115*, 4669−4671; *Angew. Chem., Int. Ed.* **2003**, *42*, 4531−4533. (d) Strohmann, C.; Strohfeldt, K.; Schildbach, D. *J. Am. Chem. Soc.* **2003**, *125*, 13672–13673. (e) Strohmann, C.; Strohfeldt, K.; Schildbach, D.; McGrath, M. J.; O'Brian, P. *Organometallics* **2004**, *23*, 5389–5391. (f) Strohmann, C.; Dilsky, S.; Strohfeldt, K. *Organometallics* **2006**, *25*, 41–44. (g) Strohmann, C.; Gessner, V. H. *Angew. Chem.* **2007**, *119*, 4650–4653; *Angew. Chem., Int. Ed.* **2007**, *46*, 4566−4569. (h) Strohmann, C.; Gessner, V. H. Angew. Chem. 2007, *119*, 8429−8431; Angew. Chem., Int. Ed. **2007**, *46*, 8281−8283. (i) Strohmann, C.; Gessner, V. H. *J. Am. Chem. Soc.* **2007**, *129*, 8952–8953.

(18) Rademacher, P. *Strukturen organischer moleküle*; VCH: New York, 1987.

Table 1. Crystallographic Data for (*R*,*S*)-**2**·Quinuclidine and (*S*,*R*,*S*)-**4**·MeI

compound	(*R*,*S*)-**2** · quinuclidine[a]	(*S*,*R*,*S*)-**4** · MeI[b]
empirical formula	$C_{23}H_{39}LiN_2OSi$	$C_{20}H_{38}INOSiSn$
CCDC no.	670562	670561
molecular mass (g mol^{-1})	394.59	582.19
temperature (K)	100(2)	173(2)
wavelength (Å)	0.71073	0.71073
crystal system	orthorhombic	orthorhombic
space group (no.)	$P2_12_12_1$ (no. 19)	$P2_12_12_1$ (no. 19)
a (Å)	9.5424(7)	8.9491(9)
b (Å)	11.2137(8)	14.9054(14)
c (Å)	21.7553(16)	18.5409(18)
V (Å^3)	2327.94(29)	2473.2(4)
Z	4	4
calculated density ρ (g cm^{-3})	1.126[b]	1.564
absorption coefficient μ (mm^{-1})	0.116[b]	2.338
F(000)	864[b]	1160
crystal dimensions (mm^3)	0.30 × 0.30 × 0.25	0.40 × 0.20 × 0.10
range of data collection 2θ (deg)	3.74−100.17	3.50−50.90
completeness to $2\theta_{max}$ (%)	99.9	100
mean redundancy to $2\theta_{max}$	10.8	8.6
reflections collected	264882	39343
independent reflections	24554 (R_{int} = 0.0228)	4588 (R_{int} = 0.0555)
refinement method	full-matrix least squares on F^2	full-matrix least squares on F^2
data/restraints/parameters	21027/0/616	4563/0/236
GOF	2.595	1.138
max shift/esd in final cycle	0.99 × 10^{-7}	1.0 × 10^{-3}
final *R* values [$I > 2\sigma(I)$]		R1 = 0.0311, wR2 = 0.0638
final *R* values [$I > 3\sigma(I)$]	R1 = 0.0203, wR2 = 0.0312	
absolute structure parameter	0.01(3)[b]	0.00(3)
largest diff. peak and hole (e Å^{-3})	0.211 and −0.134	0.894 and −0.454

[a] Values given for multipole refinement. [b] Values taken from the IAM refinement with SHELXL.

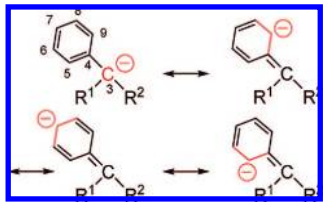

Figure 4. Mesomeric formulas of the metalated carbon atom and the phenyl substituent in (*R*,*S*)-**2**·quinuclidine.

different mesomeric formulas that have a stabilizing effect are feasible (Figure 4).

This is already obvious by looking at the bond lengths in the phenyl substituent and at the C_{ipso}−Li bond. The bond between C(3) and C(4) is significantly shortened (1.434 Å) in comparison with one between a nonmetalated benzylic carbon atom and the neighboring *ipso*-phenyl carbon atom. Nevertheless, the bond length is more in the range of a single than of a double bond (1.466 Å for a C(sp^2)−C(sp^2) single bond compared to a double bond length of 1.335 Å).[18] The C−C bond distances between the *ipso*- and the *ortho*-carbon atoms are slightly elongated (C(4)−C(5) = C(4)−C(9) = 1.427 Å) compared to C(8)−C(9) (1.390 Å) and C(5)−C(6) (1.386 Å). The two nitrogen−lithium bond lengths of 2.161 (Li−N(1)) and 2.118 Å (Li−N(2)) differ significantly. The shortened bond between the lithium and the nitrogen atom of the quinuclidine might indicate that quinuclidine is a better donor than the substituent. The latter distance might, however, be constrained by the lack of side-arm complexation flexibility.

Determination of the Stereochemical Pathway. As shown above, in principle (*R*,*S*)-**2**·quinuclidine could be attacked by electrophiles from two sides: from the front side (where the lithium atom is located) and from the open back side. To determine the reaction pathway of the whole sequence (and

Scheme 4. Synthesis of (*S*,*S*)-**4** and (*S*,*R*,*S*)-**4**·MeI

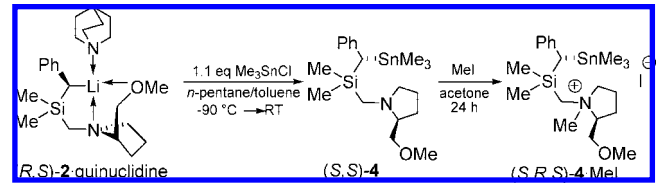

therefore the favored reaction side of (*R*,*S*)-**2**·quinuclidine for electrophiles), it was reacted with 1.1 equiv of trimethylchlorostannane at −90 °C. Warming to room temperature caused a complete decolorization of the previously yellow solution. ^{13}C NMR spectroscopic studies showed a dr of the product (*S*,*S*)-**4** of ≥98:2. Subsequent treatment of (*S*,*S*)-**4** with 1 equiv of MeI in acetone resulted in the methylated product (*S*,*R*,*S*)-**4**·MeI (Scheme 4).

In consequence, (*S*,*R*,*S*)-**4**·MeI has three stereogenic centers: two at carbon atoms and one at a nitrogen atom. Both stereogenic carbon atoms were determined to have (*S*)-configuration, and the nitrogen atom was determined to have (*R*)-configuration. The absolute configurations could be determined unambiguously on the basis of the known configuration of C(17). The refinement of the Flack *x* parameter to 0.00(3) additionally confirmed the proposed stereoisomer.[15] Hence, the trapping reaction of (*R*,*S*)-**2**·quinuclidine with trimethylchlorostannane proceeds under inversion of the absolute configuration.

(*S*,*R*,*S*)-**4**·MeI crystallizes from acetone/Et$_2$O in the orthorhombic space group $P2_12_12_1$ as colorless needles (Figure 5). The asymmetric unit contains one molecule. All angles and bond lengths of (*S*,*R*,*S*)-**4**·MeI are in the typical range seen in other benzylsilanes.[3h] Crystallographic data are presented in Table 1.

Topological Analysis of the Electron Density Distribution in (*R*,*S*)-2·Quinuclidine. Details of the data acquisition and

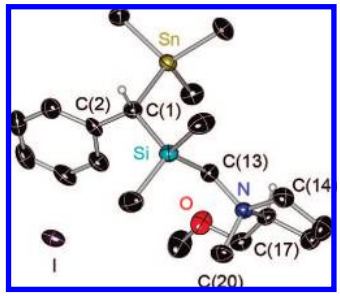

Figure 5. Molecular structure and numbering scheme of (*S*,*R*,*S*)-**4**·MeI in the solid state. Anisotropic displacement parameters are depicted at the 50% probability level. Selected bond lengths (Å) and angles (deg): C(1)−C(2), 1.508(6); C(1)−Si, 1.872(5); C(1)−Sn, 2.193(5); C(20)−N, 1.492(6); Si−C(1)−Sn, 117.5(2); C(1)−Si−C(13), 104.0(2); C(14)−N−C(13), 111.1(4); C(14)−N−C(17), 102.8(3); C(13)−N−C(17), 110.5(3).

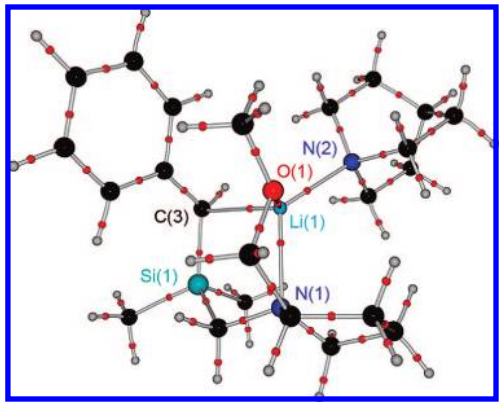

Figure 6. Molecular graph showing the determined bond paths of (*R*,*S*)-**2**·quinuclidine including chemically relevant BCPs (red).

multipole refinement are given in the Supporting Information. On the basis of our final multipole model, a complete topological analysis of the charge density was performed according to Bader's quantum theory of atoms in molecules (QTAIM).[19] This theory allows a detailed study of the chemical interactions in the compound (*R*,*S*)-**2**·quinuclidine on the basis of its experimentally determined electron density distribution. All expected bond critical points (BCPs; (3, −1) critical points in $\rho(\mathbf{r})$) in the molecule, representing saddle points in the electron density distribution between two atoms, have been found (Figure 6). According to the QTAIM, a BCP is a sufficient and necessary condition for a chemical bond between two atoms.[20] The values of the charge density, $\rho(\mathbf{r}_{BCP})$, and the Laplacian, $\nabla^2\rho(\mathbf{r}_{BCP})$, at the BCPs can be used to distinguish between various types of interactions. Negative values of the Laplacian accompanied by high electron density values at the BCPs are commonly associated with a covalent character of the bond (shared interactions), while distinct positive values of the Laplacian accompanied by low electron densities are attributed to closed-shell interactions (e.g., ionic, coordinative, metal−metal bonds).

However, it is well known that this strict classification does not hold for very polar bonds or interactions with metal atoms.[21] Nevertheless, it is an appropriate rule at least for bonds between first row elements. Moreover, the absolute value of $\rho(\mathbf{r}_{BCP})$ can be related to the bond order. This is a convincing measure for the delocalization of negative charge into the phenyl ring. Additional information can be gained by the value of the bond ellipticity, $\varepsilon(\mathbf{r}_{BCP})$ $(\lambda_1/\lambda_2 - 1)$, where the λ's are the two eigenvalues of the Hessian matrix perpendicular to the bonding vector. A value close to zero indicates a cylindrical bond shape adopted in single or triple bonds. A large $\varepsilon(\mathbf{r}_{BCP})$ is generally assigned to bonds with a distinct preference in one direction in space as it is the case for π-bonding.

The electron density values at the BCPs of the carbon−carbon bonds within the C_7-benzyl substituent (C(3) to C(9)) show the highest values observed in the whole molecule (Table 2). The mean value (2.15 e Å^{-3}) is significantly higher than the values of the carbon−carbon single bonds (range from 1.62 to 1.83 e Å^{-3}) in the complex.

In view of the aromaticity in the phenyl ring, this is not surprising. However, the aromatic part shows no increased electron density values at the BCPs compared to known systems that are not suspect to external π-interactions (experimental values range from 2.11 to 2.26 e Å^{-3}).[22] The same is true for the Laplacian, which ranges from −16.8 to −20.4 e Å^{-5} (literature: −16.0 to −20.7 e Å^{-5}) and a more or less constant ellipticity in the phenyl ring. Therefore, the influence of the deprotonated atom on the ring system is rather small according to these data.

When we focus on C(3), a different situation is found. According to Figure 4, two electronic situations are feasible for the C(3)−C(4) bond: a C−C single bond if the negative charge is located at C(3) or a partial double bond if charge delocalization into the ring system is assumed. A standard C(3)−C(4) single bond can be precluded by the topological properties $\rho(\mathbf{r}_{BCP})$ (2.02 e Å^{-3}), the Laplacian (−16.76 e Å^{-5}), and the ellipticity of 0.19 (compare ethane: $\rho(\mathbf{r}_{BCP}) = 1.62$ e Å^{-3}; $\nabla^2\rho(\mathbf{r}_{BCP}) = -13.64$ e Å^{-5}; ethene: $\rho(\mathbf{r}_{BCP}) = 2.26$ e Å^{-3}; $\nabla^2\rho(\mathbf{r}_{BCP}) = -23.83$ e Å^{-5}; ethine: $\rho(\mathbf{r}_{BCP}) = 2.66$ e Å^{-3}; $\nabla^2\rho(\mathbf{r}_{BCP}) = -27.10$ e Å^{-5}).[23] The values found reflect an intermediate situation: increased compared to a single bond but decreased with respect to the aromatic ring.

Integrated charges were determined to estimate a possible charge transfer to the benzylic unit. These physically meaningful charges can be obtained by integrating the electron density over the atomic basins separated by the zero flux surface($\nabla\rho(\mathbf{r})\cdot\mathbf{n}(\mathbf{r}) = 0$). They originate from bond *polarization* effects as well as *charge transfer* between the atoms. Strikingly, the charge at the deprotonated atom is almost −1 (−0.97 e). Summing up the atomic charges in the phenyl ring including those of the hydrogen atoms gives a charge of −0.1 e. This is why the aromatic ring does not show any features of an additionally delocalized negative charge. The charge seems to be localized mainly at C(3).

(19) Bader, R. F. W. *Atoms in molecules: A quantum theory*; Oxford University Press: New York, 1990.
(20) Bader, R. F. W. *J. Phys. Chem. A* **1998**, *102*, 7314–7323.
(21) (a) Flierler, U.; Burzler, M.; Leusser, D.; Henn, J.; Ott, H.; Braunschweig, H.; Stalke, D. *Angew. Chem., Int. Ed.* **2008**, *47*, 4321–4325. (b) Kocher, N.; Henn, J.; Gostevskii, B.; Kost, D.; Kalikhman, I.; Engels, B.; Stalke, D. *J. Am. Chem. Soc.* **2004**, *136*, 5563–5568. (c) Leusser, D.; Henn, J.; Kocher, N.; Engels, B.; Stalke, D. *J. Am. Chem. Soc.* **2004**, *126*, 1781–1793. (d) Henn, J.; Ilge, D.; Leusser, D.; Stalke, D.; Engels, B. *J. Phys. Chem. A* **2004**, *108*, 9442–9452.
(22) (a) Hibbs, D. E.; Hanrahan, J. R.; Hursthouse, M. B.; Knight, D. W.; Overgaard, J.; Turner, P.; Piltz, R. O.; Waller, M. P. *Org. Biomol. Chem.* **2003**, *1*, 1034–1040. (b) Destro, R.; Soave, R.; Barzaghi, M.; Lo Presti, L. *Chem.−Eur. J.* **2005**, *11*, 4621–4634. (c) Glukhov, I. V.; Lyssenko, K. A.; Korlyukov, A. A.; Antipin, M. Y. *Russ. Chem. Bull., Int. Ed.* **2005**, *54*, 547–559. (d) Chopra, D.; Cameron, T. S.; Ferrara, J. D.; Guru Row, T. N. *J. Phys. Chem. A* **2006**, *110*, 10465–10477. (e) Mebs, S.; Messerschmidt, M.; Luger, P. *Z. Kristallogr.* **2006**, *221*, 656–664.
(23) Macchi, P.; Sironi, A. *Coord. Chem. Rev.* **2003**, *238−239*, 383–412.

Table 2. Bond Path Length, Electron Density, Laplacian, and Ellipticity at the BCPs of (*R*,*S*)-**2**·Quinuclidine

	C(3)−C(4)	C(4)−C(5)	C(5)−C(6)	C(6)−C(7)	C(7)−C(8)	C(8)−C(9)	C(9)−C(4)
bond path (Å)	1.4369	1.4282	1.3873	1.3978	1.4005	1.3921	1.4268
$\rho(\mathbf{r}_{BCP})$ (e Å^{-3})	2.02(1)	2.12(1)	2.25(1)	2.20(2)	2.18(2)	2.22(1)	2.05(1)
$\nabla^2\rho(\mathbf{r}_{BCP})$ (e Å^{-5})	−16.76(4)	−17.89(3)	−20.39(3)	−19.13(4)	−18.18(4)	−19.85(3)	−17.48(3)
$\varepsilon(\mathbf{r}_{BCP})$	0.19	0.18	0.22	0.24	0.24	0.25	0.22

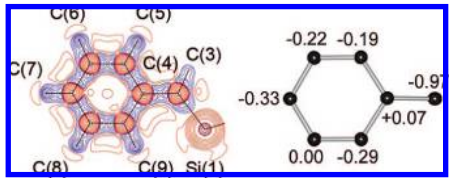

Figure 7. Laplacian distribution in the C(3)−C(6)−C(8) plane (left) and integrated charges [e] (right) of (*R*,*S*)-**2**·quinuclidine. The molecule is similarly oriented in both diagrams. Positive values of $\nabla^2\rho(\mathbf{r})$ are depicted by red and negative by blue lines. Contours are drawn at $\pm2.0 \times 10^n$, −15, −30, $\pm4.0 \times 10^n$, $\pm8.0 \times 10^n$ e Å^{-5} with $n = 0, 1, 2, 3$.

Interestingly, we find the aromatic electron density in the ring to be asymmetrically distributed. The $C_{ipso}-C_{ortho}$ bonds are significantly elongated compared to the remaining ring bonds. The electronic consequence predicted by the mesomerical structures b−d in Figure 4, as well as an inductive effect, can be rationalized at the *ortho*- and *para*-carbon atoms. They reveal distinct negative charges (−0.19, −0.29, and −0.33 e) (Figure 7). Remarkably, the negative charges are not strictly limited to the ortho and para positions, since a charge of −0.22 e is found in the meta position at C(6). This feature has an impact on the crystal packing of the donor free structure, (*R*,*S*)-**2**.[3e] Intermolecular η^2-coordination of C(7) and C(6) to a neighboring lithium atom occurs. It is noteworthy that the different atomic charges originate solely from the carbon atoms, since all the hydrogen atoms have almost the same charge (+0.17 e).

The charge generated by the deprotonation still seems to be concentrated at the carbon atom C(3), counterbalancing the charge of +0.94 e at the lithium cation. Yet, analyzing the details, the electronic situation is not straightforward. By partitioning the whole molecule into subunits (Scheme 5), we can determine their group charges. The quinuclidine donor group charge is slightly positive with +0.16 e, while the dimethylsilyl bridge contributes substantially with +1.22 e. This is mainly balanced by the benzyl (−0.87 e) and the pyrrolidine group (−1.08 e; −1.22 e contributed by N(1)) and to a small extent by the methoxy side arm (−0.39 e). This gives rise to a totally different view of the charge density distribution in (*R*,*S*)-**2**·quinuclidine. The soft Lewis acid and therefore easily polarizable silicon atom forms another cationic unit.

As mentioned in the discussion of the structural features, the Si−C(3) bond is significantly shortened compared to a standard Si−C bond as well as to the mean value of reported Si−C(sp^2) bond lengths (1.86 Å). Its bond strengthening is shown by a slightly increased $\rho(\mathbf{r}_{BCP})$ value of 0.90 e Å^{-3} compared to the other Si−C BCP values of 0.81 e Å^{-3}. This is accompanied by the highest positive Laplacian of a carbon atom bond (4.17 e Å^{-5}) in (*R*,*S*)-**2**·quinuclidine and the shortest Si−BCP distance. The expansion of the atomic basin of C(3) reflects the influence of the observed charge accumulation.

A comparison of the bond characteristics of all silicon−carbon bonds in this complex reveals very low values of the electron density at the BCPs. A halved value (0.81−0.90 e Å^{-3}) is observed compared to carbon−carbon single bonds. The $\nabla^2\rho(\mathbf{r}_{BCP})$ values are all positive resembling a silicon−carbon

Scheme 5. Subunits and Corresponding Group Charges of (*R*,*S*)-**2**·Quinuclidine

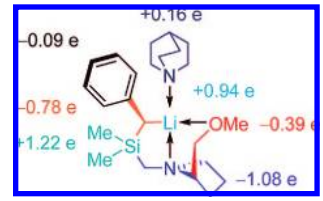

contact with ionic contributions. This is supported by the spherical shape of the charge depletion around the silicon atom (Figure 8) and the positive atomic charge of +2.15 e.[24] Even the net charge, a property mainly reflecting charge transfer phenomena, reveals a distinct positive value at the silicon atom (+1.05 e).

Moreover, the shapes of the Laplacian distribution of the bonded carbon atoms reflect polarized interactions.[21b] Obviously, the charge accumulations in the bonding regions are limited to the carbon basins. All Si−C bonds except Si(1)−C(3) reveal the same distribution. The minimum along Si(1)−C(3) is shifted toward the BCP because of the bond shortening. Nevertheless, the shape of the curve is typical for a distinctly polarized interaction with charge depletion over the whole basin of the electropositive partner and charge concentration close to the electronegative atom (Figure 8).[25]

The bond ellipticities give insight into polarization effects on the bonding characteristics. For the Si−C interactions, one can distinguish two types of $\varepsilon(\mathbf{r})$ distributions along the bond paths (Figure 9).

For the methyl carbon atoms (C(1) and C(2)), a maximum is found at the BCP, although on a very low level ($\varepsilon_{BCP} = 0.09$) and close to the value of the C−C single bond (C(13)−C(12): $\varepsilon_{BCP} = 0.07$). The two remaining Si−C bonds reveal comparably low values at the BCPs (0.08 and 0.05), but the profile of $\varepsilon(\mathbf{r})$ is different. Distinct maxima with high values are observed at the electronegative carbon atoms, while the ellipticity decreases in the proximity of Si(1) in both bonds. C(3), which shows the highest atomic charge, gives rise to the most pronounced maximum. Therefore, we assume that the bond polarization that is guided by the buildup of pronounced charges decays along the series from C(3) over C(10) to the methyl carbon atoms. An analogous inspection of Si−C bond ellipticities was performed in the pioneering work of Scherer et al. concerning Li−H agostic interactions and negative hyperconjugation.[26] The shape of $\varepsilon(\mathbf{r})$ close to the carbon atom in the picolyllithium compound is similar to the one presented here, although a clearly visible shoulder close to the BCP can be found in ref 26a. This shoulder was compared to the one of a Si−C double bond,

(24) A comparably high charge was reported in ref 21b.
(25) Kocher, N.; Selinka, C.; Leusser, D.; Kost, D.; Kahlikhman, I.; Stalke, D. *Z. Anorg. Allg. Chem.* **2004**, *630*, 1777–1793.
(26) (a) Scherer, W.; Sirsch, P.; Shorokhov, D.; McGrady, G. S.; Mason, S. A.; Gardiner, M. G. *Chem.−Eur. J.* **2002**, *8*, 2324–2334. (b) Scherer, W.; Sirsch, P.; Grosche, M.; Spiegler, M.; Mason, S. A.; Gardiner, M. G. *Chem. Commun.* **2001**, 2072–2073.

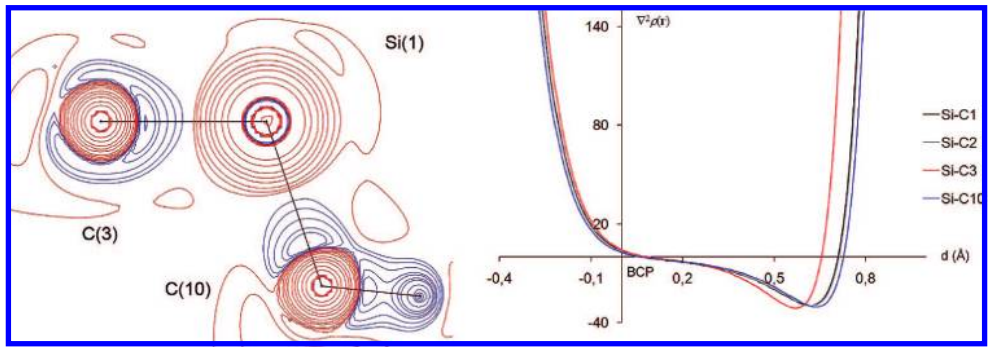

Figure 8. $\nabla^2\rho(\mathbf{r})$ in the C(3)−Si(1)−C(10) plane (left) (positive values are depicted by red and negative values by blue lines. Contours are drawn at $\pm 2.0 \times 10^n$, -15, -30, $\pm 4.0 \times 10^n$, $\pm 8.0 \times 10^n$ e Å^{-5} with $n = 0, 1, 2, 3$) and Laplacian distribution along the bond paths of the silicon−carbon interactions in (*R*,*S*)-**2**·quinuclidine (right) (basin of the silicon atom is plotted to negative distance values).

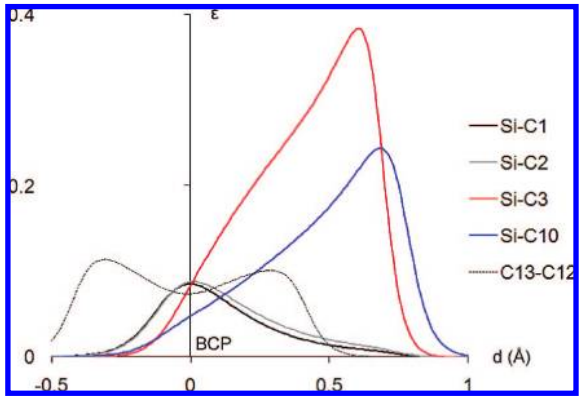

Figure 9. Bond ellipticities of silicon−carbon bonds in (*R*,*S*)-**2**·quinuclidine along the bond paths in comparison with that of C(12)−C(13); the basin of the former atom is displayed at negative distance values.

which shows a maximum in $\varepsilon(\mathbf{r})$ close to the BCP, and interpreted as a sign for a charge delocalization through negative hyperconjugation. A related pronounced feature cannot be found in (*R*,*S*)-**2**·quinuclidine. Nevertheless, negative hyperconjugation seems to play a role in stabilizing the carbanion, as could be seen from the different bond lengths of C(3)−Si(1) and C(10)−Si(1) (compare with that in Molecular Structure in the Crystal of (*R*,*S*)-**2**·Quinuclidine). The question now arising is: *What do these findings mean for the stereochemical stabilization of the deprotonated atom?*

The phenyl ring is more or less electronically undisturbed with respect to the group charge. On the other hand, the neighboring silicon atom is highly positively charged, forming a short bond to the carbon atom C(3). The stabilization is therefore accomplished by a strong electrostatic interaction caused by two distinct charges localized at the bound atoms, charge polarization, and negative hyperconjugation.[27] This is the key to understand why the C(3)−X [X = Si(1), C(4), H(3)] bonds are in one plane with a mean deviation of less than 0.04 Å. If we conclude that the Si(1)−C(3) bond is reinforced by electrostatic contributions, which can be deduced from the integrated charges (−0.97 e and +2.15 e), the planarity is the logical consequence. This leaves the elevated electron density more or less equally distributed around the silicon atom, without localization in an oriented lone pair (LP), which would concentrate negative charge further away from the silicon atom.

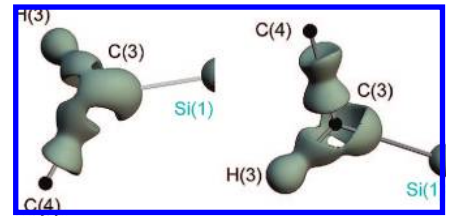

Figure 10. Isosurface map of the Laplacian distribution in (*R*,*S*)-**2**·quinuclidine around C(3) at constant $\nabla^2\rho(\mathbf{r})$ of -10 e Å^{-5}. Left: view from upper side facing Li(1). Right: opposite side.

Therefore, an ideal electrostatic interaction is accomplished. *Can this be further proven and how does that influence the reactive surface around C(3)?*

The BCP search around C(3) led to bond paths to all neighboring atoms including Li(1). A bond to the cationic atom has to be assumed. Yet, the localization of the formal negative charge at the deprotonated carbon atom remains undisclosed. In general, it is associated with a p-orbital orthogonal to the sp^2-bond plane resulting in a hypothetical lone pair. If this LP[28] interacts with the lithium atom, a polarization toward the metal atom should give a distinct valence shell charge concentration (VSCC). The second derivative of the charge density distribution, $\nabla^2\rho(\mathbf{r})$, which represents charge accumulations and depletions, was therefore analyzed for the existence of local maxima in the negative Laplacian field, $L(\mathbf{r})$. The corresponding maxima ((3, −3) critical points, VSCCs) can be separated into bonding (BCC) or nonbonding charge concentrations (NBCCs, often referred to as LPs). But even an intense VSCC search around C(3) resulted in solely three BCCs to the nonmetal atoms. No charge concentration (CC) could be detected, either facing the lithium atom or located at the back side of the benzylic group. Nevertheless, the distribution of $\nabla^2\rho(\mathbf{r})$ at a level of -10 e Å^{-5} shows a pronounced difference between the front side facing the lithium atom and the opposite side (Figure 10). Although no LP was found, the density is clearly concentrated above the shown C4−C3−Si1 plane (toward the cation) while no such concentration is visible at the opposite side.

Can one deduce a front side attack from the electron density point of view? Definitely not! The polarized electron density in the direction toward the lithium atom cannot be the driving force of an electrophilic attack. This is supported by the lack of LP density. This polarization should not be sufficient to direct an

(27) The extent of the stabilization through negative hyperconjugation could not be quantified. The torsion angle Li(1)−C(3)−Si(1)−C(10) of 32.8° is just 6° wider than the one in ref 26.

(28) Because of the bond path to the lithium atom, the nomenclature is rather wrong, but is maintained because of the common association of a deprotonated carbon atom with a lone pair.

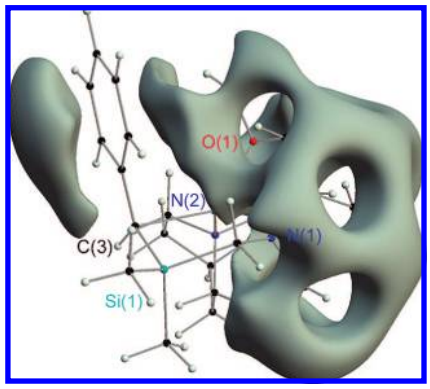

Figure 11. ESP isosurface drawn at a level of −0.1 e Å^{-1} of (*R*,*S*)-**2**·quinuclidine.

electrophile into the sterically blocked pocket near the cation. Since the solid-state structure is maintained in solution (see ^{13}C NMR Studies of (*R*,*S*)-**2**·Quinuclidine) without facilitating a reaction pathway from the front side by dissociation of (*R*,*S*)-**2**·quinuclidine, the charge distribution at the back side must be the driving force.

To visualize this, the electrostatic potential (ESP) was determined from the experimental charge density distribution. The ESP at a given point in space is defined as the work required to bring a positive charge from infinite distance to the selected point and is therefore suitable for studying chemical reactivity. Figure 11 shows the ESP at a level of −0.1 e Å^{-1}. Two areas for a possible electrophilic attack can be identified. The first covers the pyrrolidine ring including the methoxy side arm. This is irrelevant for a substitution reaction since an appropriate center of attack is lacking. The second area is located at the benzylic unit opposite the lithium atom. This surface is extended toward C(3). Electrophiles seem to be literally guided to the reactive center. The result of the examination of the ESP together with steric demand arguments explains in a straightforward way the observed back side attack with inversion of the stereogenic center with high diastereomeric ratios.

The interactions to the lithium atom are also of special interest. The nature of the lithium−carbon bond has been discussed controversially for more than 20 years and still is the subject of constant debate.[17,29] Charge density studies are an effective tool to classify such bonds.[30] An intramolecular bond comparison can provide unequivocal evidence with respect to the bonding situation. The nature of the lithium−oxygen bond is commonly accepted to be predominantly ionic. Therefore, the lithium−carbon bond characteristics should be compared to the observed Li−O distribution.

The positive values of $\nabla^2\rho(\mathbf{r})$ at the BCPs (Table 3) indicate a predominantly closed shell interaction for all contacts to the lithium cation. For comparison purposes, the Laplacian distribution between C(12)−C(13) is shown in Figure 12 as a paradigmatic covalent homoatomic bond: $\nabla^2\rho(\mathbf{r})$ along C(12)−C(13) shows distinct charge concentrations in the bonding region

Table 3. Bond Path Length, Electron Density, and Laplacian at the BCPs of the X−Li(1) Bonds and CC's toward Li(1) in (*R*,*S*)-**2**·Quinuclidine

	C(3)−Li(1)	O(1)−Li(1)	N(1)−Li(1)	N(2)−Li(1)
bond path (Å)	2.2789	1.9825	2.1639	2.1180
$\rho(\mathbf{r}_{BCP})$ (e Å^{-3})	0.086(2)	0.150(1)	0.113(1)	0.131(1)
$\nabla^2\rho(\mathbf{r}_{BCP})$ (e Å^{-5})	2.166(1)	4.804(1)	3.225(1)	3.700(1)
$\nabla^2\rho(\mathbf{r}_{CC})$		−133.081(32)	−73.015(20)	−74.709(19)

with a minimum between the two atoms formed on negative values of the Laplacian distribution. In contrast, $\nabla^2\rho(\mathbf{r})$ along the bond paths of the N/C−Li(1) bonds shows charge depletion within the whole bond region and qualitatively the same shape. Only the charge concentrations that are found in close proximity to the electronegative bonding partners differ in the absolute heights. In the basin of the lithium cation no VSCC can be observed, which is a prominent indicator for an ionic interaction.

An even more pronounced charge separation is adopted by the Li(1)−O(1) contact. $\nabla^2\rho(\mathbf{r})$ shows a maximum when approaching the valence shell of the oxygen atom, where it forms an extremely pronounced minimum, typical for a lone pair driven charge concentration.

With these findings, we currently conclude that the lithium−carbon bond belongs in the group of ionic metal−atom interactions showing comparable characteristics at lower absolute values to the nitrogen donor atoms and even similarities to the Li−O contact.

As mentioned above, all bond paths to the four donor sites were quantified (Table 3). Interestingly, the electron density values are related to the donor capacity. The oxygen−lithium contact is the shortest, leading to the highest electron density value of 0.15 e Å^{-3}. This is supported by the highest atomic charge (−1.32 e) and the most distinct charge CC of −133.08 e Å^{-5}. Only three VSCCs were found at the oxygen atom. Two BCCs were directed toward the carbon atoms, and one CC was oriented to Li(1) forming an acute Li−O−CC angle of 51.3°. The shape of the Laplacian distribution with a value of −100 e Å^{-5} shows that the density of the two lone pairs cannot be resolved (Figure 13).

They form a banana-shaped belt facing the metal. This effect is well known and currently interpreted as a reorientation of the LPs toward the acceptor site, thus strengthening their donating capacity.[21c,25,31]

The nitrogen atoms share almost the same values of the atomic charge (−1.13 and −1.22 e) and of the Laplacian at

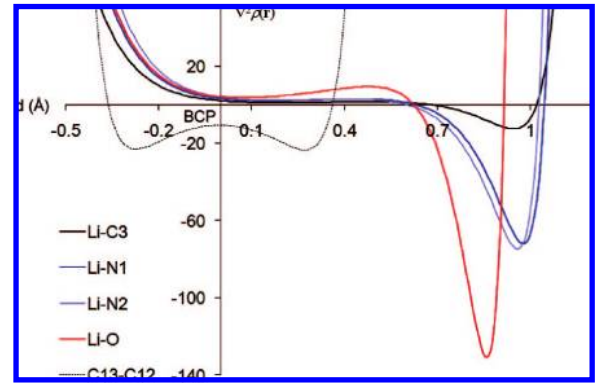

Figure 12. Laplacian distribution along the bond paths of the given lithium−donor interactions in (*R*,*S*)-**2**·quinuclidine and along a single bond as an example of a covalent bond; basin of the first mentioned atom is plotted to negative distance values.

(29) (a) Streitwieser, A.; Bachrach, S. M.; Dorigo, A.; Schleyer, P. v. R. Bonding, Structures and Energies in Organolithium Compounds. In *Lithium chemistry: A theoretical and experimental overview*; Sapse, A.-M., Schleyer, P. v. R., Eds.; Wiley & Sons: New York, 1995; pp 1−43. (b) Matito, E.; Poater, J.; Bickelhaupt, F. M.; Solà, M. *J. Phys. Chem. B* **2006**, *110*, 7189–7198. (c) Bickelhaupt, F. M.; Solà, M.; Guerra, C. F. *J. Chem. Theory Comput.* **2006**, *2*, 965–980.

(30) Deuerlein, S.; Leusser, D.; Flierler, U.; Ott, H.; Stalke, D. *Organometallics* **2008**, *27*, 2306–2315.

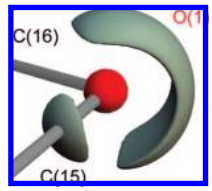

Figure 13. Laplacian distribution around O(1) on an isosurface value of −100 e Å^{-5} in (*R*,*S*)-**2**·quinuclidine.

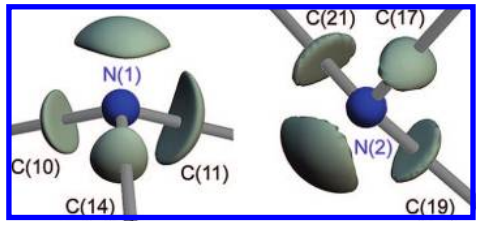

Figure 14. Laplacian distribution around N(1) and N(2) on an isosurface value of −50 e Å^{-5} in (*R*,*S*)-**2**·quinuclidine.

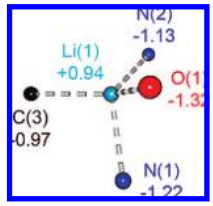

Figure 15. Integrated atomic charges of Li(1) and its coordination sphere [e] in (*R*,*S*)-**2**·quinuclidine.

their LPs (−73.02 and −74.70 e Å^{-5}) (Figure 14), but their bond lengths differ by 0.044 Å. Therefore, a lower density $\rho(\mathbf{r}_{BCP})$ is observed for the longer bond (0.11 e Å^{-3}) compared to that of N(2)−Li(1) (0.13 e Å^{-3}). In the picolyllithium compound of Scherer et al., a higher electron density value at the BCP of the pyridine−nitrogen−lithium bond was found (0.22 e Å^{-3}), which is probably due to the shorter bond length (1.9508 Å).[26]

The least prominent interaction was determined for C(3)−Li(1). This is expressed by an electron density of 0.09 e Å^{-3} at the BCP, the largest bond length (2.273(1) Å), and the absence of LP density at C(3). Moreover, this trend of decreasing donor capacity is reflected by an elongated bond path length. While the two stronger interactions (O(1) and N(2)) show no deviation of bond distance and path length, the weaker bonds are more curved (difference 0.002 Å for N(1) and 0.007 Å for C(3)). The density values can be compared to the only published experimental charge density investigation of an alkyllithium compound by Scherer et al.[26] In this picolyllithium compound, a $\rho(\mathbf{r}_{BCP})$ value of 0.150 e Å^{-3} and a $\nabla^2\rho(\mathbf{r}_{BCP})$ value of 5.201 e Å^{-5} was found for the Li−C bond, which are slightly higher than the ones in (*R*,*S*)-**2**·quinuclidine. This originates from the electronic differences at the deprotonated carbon atom. The bond length is much shorter, and a discrete CC toward the lithium atom was found.

Remarkably, the surrounding atoms of the positive lithium atom in (*R*,*S*)-**2**·quinuclidine display distinct negative atomic charges (−0.96 to −1.32 e) (Figure 15).

Each donor site equalizes the total charge at Li(1), thus leading to a strong polarization at all atoms bound to the cation. This charge accumulation is one argument for the stability of this complex. The lithium atom is fixed in a pocket of pronounced electron density. This might be the reason why the absolute structure is maintained even in solution.

Conclusions

Starting from a highly enantiomerically enriched benzylsilane, (*R*,*S*)-**2**·quinuclidine could be obtained. The absolute configuration at the metalated carbon atom C(3) of this monomeric α-lithiated compound was determined by X-ray diffraction analysis. Additional ^{13}C NMR studies were undertaken to elucidate the structure in solution. Only one quartet was found in the ^{13}C NMR spectrum for the coupling between carbon and lithium, indicating a fixed lithium−carbon contact at room temperature. After reaction of (*R*,*S*)-**2**·quinuclidine with trimethylchlorostannane, the trapped product (*S*,*S*)-**4** was obtained with a dr ≥ 98:2. On the basis of the derivative (*S*,*R*,*S*)-**4**·MeI, its absolute configuration could be determined. The reaction sequence at the lithiated carbon atom thus took place under inversion of the configuration at C(3).

Several questions of the electronic situation in (*R*,*S*)-**2**·quinuclidine could be answered by the topological analysis of the charge density. The influence of the phenyl ring with respect to the stabilization of the negative charge at C(3) was surprisingly less significant than expected. Yet, the neighboring silicon atom proved to counterbalance the charge accumulation at the deprotonated atom by a distinct positive charge. Therefore, the α-effect of the silicon atom is not just caused by a polarization of the electron density but also by an electrostatic bond reinforcement. The stereochemical course of the electrophilic substitution under inversion could be well understood by the charge density distribution in the organolithium compound. Furthermore, the lithium−carbon bond was verified and could be integrated consistently into the set of other polar donor bonds.

Experimental Section

Experimental Procedures. All reactions were carried out under an argon atmosphere using Schlenk tubes. The solvents, including the NMR solvents, were dried according to common procedures. All NMR spectra were measured on a Bruker DRX-300 NMR spectrometer. Assignment of the signals was supported by DEPT-135- and C,H COSY experiments and the relative intensities of the resonance signals. If not indicated otherwise, each carbon signal stands for one carbon atom in the spectra.

The crystals were mounted at −100 °C (N_2 stream), using the X-TEMP 2 device.[32] The structure determination of (*R*,*S*)-**2**·quinuclidine was performed on a Bruker TXS-Mo rotating anode with INCOATEC Helios mirror optics and APEX II detector. The APEX2 v2.0−2 software (Bruker AXS, 2005) was used for the data collection and cell determination, while SAINT v7.23A (Bruker, 2005) was used for the integration and cell refinement. The numerical absorption correction and the merging of the data were achieved with SADABS-2006/3 (Sheldrick, 2006). The crystal structure determination of (*R*,*S*,*S*)-**4**·MeI was performed on a Bruker APEX-CCD (D8 three-circle goniometer). The data collection, cell determination, and refinement were achieved with SMART version 5.622 (Bruker AXS, 2001); integration: SAINT v7.36A (Bruker, 2006); empirical absorption correction: SADABS-2007/5 (Sheldrick, 2007). Both structures were solved and refined using SHELXTL.[33] Crystallographic data (excluding structure factors) were deposited with the Cambridge Crystallographic Data Centre as

(31) Kocher, N.; Leusser, D.; Murso, A.; Stalke, D. *Chem.−Eur. J.* **2004**, *10*, 3622–3631.

(32) (a) Kottke, T.; Stalke, D. *J. Appl. Crystallogr.* **1993**, *26*, 615–619. (b) Stalke, D. *Chem. Soc. Rev.* **1998**, *27*, 171–178.

(33) Sheldrick, G. M. *Acta Crystallogr.* **2008**, *A64*, 112–122.

supplementary publication no. listed in Table 2. Copies of the data can be obtained free of charge on online application to the CCDC.

(*R*,*S*)-2·Quinuclidine. A solution of [(*S*)-2-(methoxymethyl)pyrrolidinomethyl]dimethyl benzylsilane [(*S*)-**1**; 450 mg, 1.62 mmol] and quinuclidine (154 mg, 1.62 mmol), dissolved in 10 mL of *n*-pentane, was combined with 950 μL (1.62 mmol) of a solution of *t*-BuLi in *n*-pentane (1.7 M) at −90 °C. Upon warming to room temperature, the lithium compound [(*R*,*S*)-**2**]·quinuclidine was obtained as a yellow powder. By addition of about 1.5 mL of toluene, the precipitate was redissolved and the resulting yellow solution was kept at −30 °C. After 24 h, yellow rhombohedral crystals of [(*R*,*S*)-**2**]·quinuclidine were obtained, suitable for X-ray structural analysis (yield: 608 mg, 1.54 mmol, 95%). ^{1}H NMR (300.1 MHz, $C_6D_5CD_3$): δ 0.24 (s, 3H; SiCH_3), 0.40 (s, 3H; SiCH_3), 1.15−1.25 [m, 6H; N(CH_2CH_2)$_3$], 1.30−1.50 (m, 4H; $NCH_2CH_2CH_2$ and 1H; SiCH_2N and 1H; NCH_2CH_2CH), 1.81 (broad, 1H; SiC*H*Li), 1.85−2.05 (m, 1H; NC*H* and 1H; $NCH_2CH_2CH_2$), 2.55−2.65 [m, 6H; N(CH_2CH_2)$_3$ and 1H; SiCH_2N and 3H; OCH_3], 2.71 (ABX system, unresolved, 1H; CH_2O), 2.95−3.10 (m, 1H; $NCH_2CH_2CH_2$), 3.35 (ABX system, unresolved, 1H; CH_2O), 6.65−7.05 ppm (m, 5H; C_6H_5). {1H}^{13}C NMR (100.6 MHz, $C_6D_5CD_3$): δ −2.25, 0.72 (1C each) (SiCH_3), 20.5 (NCH_2CH_2CH), 22.2 ($NCHCH_2CH_2$), 26.1 (3C) [N(CH_2CH_2)$_3$], 26.6 (NCH_2CH_2), 36.5 ($^1J_{C,7\text{-}Li}$ = 9 Hz; Si*C*HLi), 47.6 (3C) [N(CH_2CH_2)$_3$], 48.1 (SiCH_2N), 57.9 (NCH_2CH_2), 58.3 (OCH_3), 67.7 (N*C*H), 70.3 (CH_2O), 108.5 (*C*-*p* of C_6H_5], 127.9, 128.8 (4C) (*C*-*o* and *C*-*m* of C_6H_5), 157.6 ppm (*C*-*i* of C_6H_5). {1H}^{29}Si NMR (59.6 MHz, $C_6D_5CD_3$): δ −13.7 ppm. {1H}^{7}Li NMR (116.6 MHz, $C_6D_5CD_3$): δ 0.48 ppm.

(*S*,*S*)-4. A solution of [(*S*)-2-(methoxymethyl)pyrrolidinomethyl]dimethyl benzylsilane [(*S*)-**1**; 450 mg, 1.62 mmol] in 10 mL of *n*-pentane was combined with 950 μL (1.62 mmol) of a solution of *t*-BuLi in *n*-pentane (1.7 M) at −90 °C. After five minutes at −90 °C, the solution was allowed to warm to room temperature and stirred for 3 h. Thereupon, 1.1 equiv of Me_3SnCl (355 mg, 1.78 mmol) were added at −90 °C, and the solution was allowed to warm to room temperature again. After removal of all volatiles in vacuo, the resulting oil was dissolved in 5 mL of *n*-pentane and separated of all salts. Finally, the crude product was cleaned through bulb-to-bulb distillation (oven temperature: 115 °C, pressure: 1.6×10^{-5} mbar; yield: 510 mg, 1.16 mmol, 71%). dr ≥ 98:2. ^{1}H NMR (300.1 MHz, $CDCl_3$): δ −0.03 (s, 3H; SiCH_3), 0.02 (s, 3H; SiCH_3), 0.06 (s, $^2J_{H,117\text{-}Sn}$ = 25.1 Hz, $^2J_{H,119\text{-}Sn}$ = 26.2 Hz, 9H; SnCH_3), 1.85 (broad, 1H; SiC*H*Sn), 1.44−1.90 (m, 4H; CH_2), 1.64, 2.51 (AB system, $^2J_{AB}$ = 13.7 Hz, 2H; SiCH_2N), 1.95−2.17 (m, 1H; CH_2), 2.29−2.34 (m, 1H; CH_2), 2.92−3.15 (m, 1H; NCH_2C), 3.06−3.15 (m. 1H; CH_2O), 3.28 (m, 3H; OCH_3), 3.33−3.48 (m, 1H; CH_2O), 6.90−7.22 ppm (m, 5H; C_6H_5). {1H}^{13}C NMR (75.5 MHz, $CDCl_3$): δ −8.1 (6C, D1 = (*S*,*S*)-**4** + D2 = (*R*,*S*)-**4**) ($^1J_{C,117\text{-}Sn}$ = 155.9 Hz, $^1J_{C,119\text{-}Sn}$ = 163.2 Hz; SnCH_3), −1.4 (D2), −1.0 (D1), −0.9 (D1), −0.5 (D2) (1C each) (SiCH_3 each), 14.1 (D1), 14.11 (D2) (1C each) (Si*C*HSn), 23.1 (D2), 23.2 (D1), 28.3 (D2), 28.4 (D1) (NCH_2CH_2C, $NCHCH_2C$), 45.7 (SiCH_2N), 57.4 (D2), 57.5 (D1) (NCH_2C), 58.9 (D1), 59.1 (D2) (OCH_3), 67.6 (D1), 67.7 (D2) (N*C*H), 76.4 (D1), 77.2 (D2) (OCH_2), 122.7 (*C*-*p* of C_6H_5), 128.1 (2C) (*C*-*o* or *C*-*m* of C_6H_5), 128.3 (2C) (*C*-*o* or *C*-*m* of C_6H_5), 144.5 (D1), 144.6 ppm (D2) (*C*-*i* of C_6H_5). {1H}^{29}Si NMR (59.6 MHz, $CDCl_3$): δ 0.6 ppm. CHN analysis, calcd: C, 51.8; H, 8.0; N, 3.2. Found: C, 51.6; H, 7.8; N, 3.4.

(*S*,*R*,*S*)-4·MeI. An amount of 16.1 mg (113 μmol) of MeI was added to a solution of 50.0 mg (113 μmol) of (*S*,*S*)-**4** in 2 mL of acetone, and the mixture was stirred for 24 h. Afterward, all volatiles were removed in vacuo and the remaining white solid was dissolved in a little acetone. The diffusion-controlled crystallization was successful using Et_2O. After two days, a colorless crystalline solid could be obtained (yield: 54.2 mg, 93.1 μmol, 86%). ^{1}H NMR (300.1 MHz, $CDCl_3$): δ 0.10 (s, $^2J_{H,117\text{-}Sn}$ = 25.4 Hz, $^2J_{H,119\text{-}Sn}$ = 26.4 Hz, 9H; SnCH_3), 0.43 (s, 3H; SiCH_3), 0.45 (s, 3H; SiCH_3), 1.85−1.92 (m, 1H; NCH_2CH_2 and $NCHCH_2$), 1.97 (s, 1H; Si*C*HSn), 2.05−2.20 (m, 3H; NCH_2CH_2 and $NCHCH_2$), 2.81 (s, 3H; NCH_3), 3.17 (m, 3H; OCH_3), 3.50−3.55 (m, 5H; CH_2O), 3.55−3.60 (m, 1H; NCH_2C), 3.61 (AB system, $^2J_{AB}$ = 14.9 Hz, 2H; SiCH_2N), 3.75−3.85 (m, 1H; NCH_2C), 4.05−4.12 (m, 1H; NC*H*), 6.87−6.92 (m, 2 H; *H*-*o* or *H*-*m*), 7.00−7.05 (m, 1H; *H*-*p*), 7.18−7.23 ppm (m, 2 H; *H*-*o* or *H*-*m*). {1H}^{13}C NMR (125.8 MHz, $CDCl_3$): δ −8.1 (3C) ($^1J_{C,117\text{-}Sn}$ = 159.6 Hz, $^1J_{C,119\text{-}Sn}$ = 167.8 Hz; SnCH_3), 0.74, 0.83 (1C) (SiCH_3 each), 20.5, 23.6 (1C each) (NCH_2CH_2C and $NCHCH_2C$), 22.8 (1C) (Si*C*HSn), 46.5 (1C) (NCH_3), 57.3 (SiCH_2N), 59.1 (1C) (OCH_3), 68.0 (1C) (NCH_2C), 68.9 (1C) (OCH_2), 77.6 (1C) (N*C*H), 123.8 (1C) (*C*-*p* of C_6H_5], 127.6 (2C) (*C*-*o* or *C*-*m* of C_6H_5), 129.1 (2C) (*C*-*o* or *C*-*m* of C_6H_5), 142.8 ppm (1C) (*C*-*i* of C_6H_5). {1H}^{29}Si NMR (59.6 MHz, $CDCl_3$): δ −0.44 ppm. CHN analysis, calcd: C, 41.3; H, 6.6; N, 2.4. Found: C, 40.8; H, 6.5; N, 2.4.

Acknowledgment. We are grateful to the Institut für Anorganische Chemie der Universität Würzburg, the Georg-August Universität Göttingen, the Priority Program 1178 "Experimental Charge Density as the Key to Understand Chemical Interaction" of the Deutsche Forschungsgemeinschaft, the Volkswagen Stiftung (D.S.), and the Fonds der Chemischen Industrie (C.S., H.O.) for financial support. Furthermore, we acknowledge Wacker-Chemie AG and Chemetall GmbH for providing us with special chemicals. C.D. thanks the Studienstiftung des deutschen Volkes for a doctoral scholarship.

Supporting Information Available: Description of the data acquisition, multipole refinements, definition of the local coordinate systems, quality criteria after multipole refinement, Hirshfeld test, residual densities, monopole populations (and contraction/expansion parameters), critical points not discussed in the article, VSCC properties, and integration of the atomic basins, and CIF files. This material is available free of charge via the Internet at http://pubs.acs.org.

JA711104Q